

UC Irvine

UC Irvine Previously Published Works

Title

A multiscale hybrid mathematical model of epidermal-dermal interactions during skin wound healing.

Permalink

<https://escholarship.org/uc/item/0j187192>

Journal

Experimental dermatology, 28(4)

ISSN

0906-6705

Authors

Wang, Yangyang
Guerrero-Juarez, Christian F
Qiu, Yuchi
[et al.](#)

Publication Date



2019-04-01

DOI

10.1111/exd.13909

Peer reviewed

A multiscale hybrid mathematical model of epidermal-dermal interactions during skin wound healing

Yangyang Wang^{1,2,3} | Christian F. Guerrero-Juarez^{1,2,3,4,5}  | Yuchi Qiu^{1,2,3} |
Huijing Du⁶ | Weitao Chen⁷ | Seth Figueroa^{1,2,3} | Maksim V. Plikus^{1,2,4,5} |
Qing Nie^{1,2,3,5} 

¹NSF-Simons Center for Multiscale Cell Fate Research, University of California, Irvine, Irvine, California

²Center for Complex Biological Systems, University of California, Irvine, Irvine, California

³Department of Mathematics, University of California, Irvine, Irvine, California

⁴Sue and Bill Gross Stem Cell Research Center, University of California, Irvine, Irvine, California

⁵Department of Developmental and Cell Biology, University of California, Irvine, Irvine, California

⁶Department of Mathematics, University of Nebraska-Lincoln, Lincoln, Nebraska

⁷Department of Mathematics, University of California, Riverside, Riverside, California

Correspondence

Maksim V. Plikus and Qing Nie, Department of Developmental and Cell Biology, University of California, Irvine, Irvine, CA. Emails: plikus@uci.edu; qnie@uci.edu

Funding information

NSF, Grant/Award Number: DMS1562176 and DMS1763272; Pew Charitable Trust grant; NIH, Grant/Award Number: R01-AR067273, R01-AR069653, R01-GM123731, R01-NS095355 and U01-AR073159; Simons Foundation Grant, Grant/Award Number: 594598

Abstract

Following injury, skin activates a complex wound healing programme. While cellular and signalling mechanisms of wound repair have been extensively studied, the principles of epidermal-dermal interactions and their effects on wound healing outcomes are only partially understood. To gain new insight into the effects of epidermal-dermal interactions, we developed a multiscale, hybrid mathematical model of skin wound healing. The model takes into consideration interactions between epidermis and dermis across the basement membrane via diffusible signals, defined as activator and inhibitor. Simulations revealed that epidermal-dermal interactions are critical for proper extracellular matrix deposition in the dermis, suggesting these signals may influence how wound scars form. Our model makes several theoretical predictions. First, basal levels of epidermal activator and inhibitor help to maintain dermis in a steady state, whereas their absence results in a raised, scar-like dermal phenotype. Second, wound-triggered increase in activator and inhibitor production by basal epidermal cells, coupled with fast re-epithelialization kinetics, reduces dermal scar size. Third, high-density fibrin clot leads to a raised, hypertrophic scar phenotype, whereas low-density fibrin clot leads to a hypotrophic phenotype. Fourth, shallow wounds, compared to deep wounds, result in overall reduced scarring. Taken together, our model predicts the important role of signalling across dermal-epidermal interface and the effect of fibrin clot density and wound geometry on scar formation. This hybrid modelling approach may be also applicable to other complex tissue systems, enabling the simulation of dynamic processes, otherwise computationally prohibitive with fully discrete models due to a large number of variables.

KEYWORDS

epidermal-dermal interaction, fibroblast, immune cells, multiscale model, scar

1 | INTRODUCTION

Skin functions as a vital interface between organism and its environment. When injured, skin rapidly heals via a wound healing programme characterized by four distinct yet overlapping phases: hemostasis, inflammation, proliferation and remodelling^{1,2}. The primary goal of this repair programme is to re-establish barrier function by reforming stratified epidermis and restoring dermal tissue integrity^{3,4}. During the remodelling phase, regeneration of new hair follicles^{5–8} and adipose tissue^{9,10} can also take place. Cellular or molecular defects during any of these phases can lead to pathological wound healing outcomes.

Molecular composition and high-order structure of collagen bundles laid by wound fibroblasts determine the architecture and the “quality” of the dermal scar, and collagen deposition is tightly regulated by paracrine, autocrine and mechanical signals¹¹. While collagen architecture of normal skin is intricate and weave-like, scars typically have “less desirable” highly parallel collagen^{12,13}. Epidermal keratinocytes can signal to dermal fibroblasts to decrease collagen production¹⁴, while direct contact between two cell types stimulates keratinocyte proliferation and migration during wound re-epithelialization¹⁵. Epidermal-dermal crosstalk occurs via signalling growth factors¹⁶, and, for example, both wound keratinocytes and fibroblasts secrete transforming growth factor beta (TGF β) ligands, the key wound healing mediators^{17–19}. TGF β 1 is also abundant in the platelet-rich fibrin clot and has been linked to excessive extracellular matrix (ECM) deposition²⁰. This suggests that together with keratinocytes, fibroblasts and immune cells, fibrin clot serves as an important signalling centre during wound repair. While multiple lines of evidence point towards the importance of signalling crosstalk between key cellular and molecular components of the wound, the overall logic of these interactions during scar formation remains incompletely understood.

Mathematical modelling offers a useful approach to study principles of wound healing. In the past, reaction-diffusion model has been implemented to study biochemical regulation of cell cycle in the epidermis during wound re-epithelialization²¹. Another study implemented hybrid model to study how collagen fibres organize during wound healing and their role in scarring^{22,23}. The Cellular Potts model also has been used to investigate sprouting and branching during angiogenesis²⁴ and, more recently, to examine proliferation and migration of skin wound fibroblasts²⁵.

While the crosstalk between keratinocytes and fibroblasts via soluble signalling factors has been previously analysed using a continuum model²⁶, epidermal and dermal compartments were treated as one spatially homogeneous region, without taking into consideration their interactions and other important anatomical aspects of the skin. A finite element method also has been used to study interactions between keratinocytes, fibroblasts and endothelial cells²⁷. Although important, this method did not account for the interface between epidermis and dermis and, instead, modelled both of these distinct skin compartments as a continuum. Unlike dermis, epidermis

consists only of a few layers of densely packed cells, and its discrete nature likely introduces important biological effects that cannot be captured by a continuum model.

To simulate interactions between individual cells within spatially distinct epidermis and dermis and their effects on scarring, we developed an optimized two-dimensional, multiscale hybrid model of wound healing. This model incorporates dynamically continuous epidermal-dermal interface, and allows studying individual proliferating and migrating keratinocytes using discrete single-cell model, and dermal fibroblast functions using continuum model. Our simulations predict that both dermal and epidermal signalling factors are necessary to sustain steady-state ECM levels in normal skin, and to regulate new ECM deposition after wounding. Our model also predicts that high-density fibrin clot, serving as the source for signalling factors, can induce formation of raised hypertrophic scars, whereas low-density fibrin clot has the opposite effect. Finally, the model predicts causal relationships between initial wound width and depth and scarring outcomes.

2 | METHODS

The two-dimensional, multiscale hybrid mathematical model consists of two submodels allocated on two separate homogeneous regions: the dermal (*D*) and epidermal (*E*) regions. Each region is distinct and was modelled with a dynamic interface between them, termed Ω . Epidermal cells in *E* were modelled individually to evaluate their signal production and proliferation and migration abilities. In contrast, dermal fibroblasts, immune cells, ECM (including collagen bundles), and signals produced by cell types not explicitly accounted for (such as vascular cells) were modelled in a continuum.

2.1 | Discrete model on epidermal cell dynamics using subcellular element method

Epidermal keratinocytes were modelled individually through a linear cell lineage composed of basal, spinous and granular layer keratinocytes. Following our previous work²⁸, a selective differential cell adhesion mechanism was implemented to allow for proper layer stratification. Individual cells and their divisions were modelled by a subcellular element method²⁹ that has been adapted to specifically study epidermis³⁰ (see Appendix S1).

2.2 | Continuum model on signalling and dermal components

Extracellular matrix deposition and diffusive signalling molecules in both dermis and epidermis were modelled by reaction-diffusion differential equations. Dermal fibroblasts and immune cells were modelled using the Keller-Segel model³¹, which includes reaction-diffusion-advection equations controlling their diffusion, chemotactic movement, self-renewal and decay.

2.3 | Coupling of discrete and continuum models with dynamic interface

We modelled epidermal basement membrane as a dynamic interface (Ω) to separate the dermis and epidermis and used the movement of such interface to mimic dermal scar formation dynamics during wound healing. The dynamic nature of the interface is implicitly modelled by the level set method³² (see Appendix S1).

3 | RESULTS

3.1 | A multiscale model with a dynamic interface and epidermal-dermal interactions

We constructed a two-dimensional, multiscale mathematical model composed of a hybrid epidermal-dermal interface to explore the mechanisms that regulate aspects of skin physiology during homeostasis and after wounding. Epidermis (E) was modelled individually with discrete keratinocytes, whereas dermis (D) was modelled in a continuum and considers diffusive signals produced by keratinocytes, dermal fibroblasts, immune cells and other skin cells not explicitly accounted for (see Methods). Both compartments were modelled independently and separated by a dynamic interface, termed Ω . During wound healing, ECM production and fibroblast proliferation are known to be regulated by multiple signalling factors^{33–37}. Key signalling factors involved in wound healing are members of the TGF pathway, although their effects are complex. While TGF β 1 promotes collagen synthesis^{33,38}, TGF β 3 shows downregulating effects^{34,39}. Both fibroblasts and keratinocytes secrete TGF β 1³⁵, and fibroblasts respond to TGF β 1 by proliferating³⁶. This suggests that TGF β 1 serves an activator for fibroblast proliferation and ECM production, whereas TGF β 3 works as an inhibitor of ECM production. Signalling factors belonging to canonical WNT^{40–43} and PDGF pathways^{37,44–46} also regulate fibroblast activity and can serve the role of activators and inhibitors in the model.

To systematically study the role of putative regulatory signals during scar formation, we modelled diffusive signals as activator (A) and inhibitor (I). A and I assume specific roles in our model—A promotes fibroblast proliferation and ECM production, whereas I inhibits ECM production. The model obeys three basic conditions (Figure 1). First, both basal epidermal keratinocytes and dermal fibroblasts produce A and I. Immune cells can also produce A. Second, A and I diffuse through the dermis, and their production rates are directly regulated by fibroblast density and ECM production. Production of A by immune cells is regulated by their activation state, which they enter when local A signalling levels are high and above a set threshold. Third, A positively regulates ECM production, while I does the opposite. These processes are modelled in a continuum and assume the following sets of partial differential equations:

$$\frac{\partial F}{\partial t} = \nabla(D_F \nabla F - v_F F \nabla p_1) + f_F(F, p_2) - d_F F \quad (1)$$

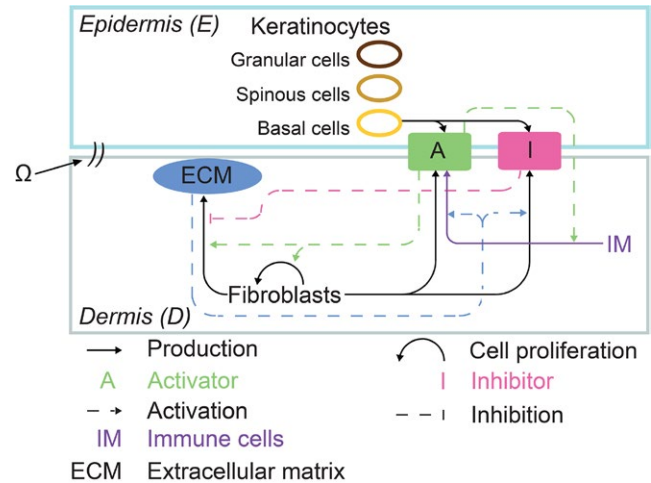


FIGURE 1 Schematic of two-dimensional multiscale hybrid model of wound healing. The modelling domain is separated into epidermis (E) (light blue) and dermis (D) (grey) by a dynamic interface (Ω) to mimic the basement membrane. In E , keratinocytes are modelled discretely as basal (yellow), spinous (light brown) and granular (dark brown) cells. Basal cells are set to produce activators A (shaded green box) and inhibitors I (shaded dark pink box) (rule (1)). In D , fibroblasts, ECM (shaded blue oval) and immune cells (IM, purple) are modelled in a continuum, where fibroblasts produce A and I, immune cells produce A, and these processes are directly activated by ECM (rule (2)). Additionally, fibroblast proliferation is activated by A, production of A by immune cells is activated by A, and ECM production is activated by A and inhibited by I (rule (3)). A and I exist in both D and E and can diffuse across Ω

$$\frac{\partial C}{\partial t} = D_C \Delta C + f_C(F, p_1, p_2) - d_C C \quad (2)$$

$$\frac{\partial p_1}{\partial t} = D_{p_1} \Delta p_1 + f_{p_1}(F, C, p_1) + E_{p_1} + C_{M p_1} M - d_{p_1} p_1 \quad (3)$$

$$\frac{\partial p_2}{\partial t} = D_{p_2} \Delta p_2 + f_{p_2}(F, C, p_2) + E_{p_2} + C_{M p_2} M + f_{IM}(IM, p_2) - d_{p_2} p_2 \quad (4)$$

where F and C represent fibroblast proliferation/density and overall ECM concentration (measured as a direct readout of collagen bundle production/deposition), respectively; p_1 and p_2 represent the concentrations of I and A, respectively. The term E_{p_i} represents the production rate of p_i (where $i = 1, 2$ in epidermal basal keratinocytes, and IM represents immune cells, which also serves as a source of A (see Appendix S1). M represents fibrin clot, which forms during wound healing (see Appendix S1).

The dynamic interface between E and D was implicitly modelled by the level set method and implemented by the phase function ϕ , which was determined by the velocity field v . The change in phase function ϕ was defined by:

$$\frac{\partial \phi}{\partial t} = -v \cdot \nabla \phi \quad (5)$$

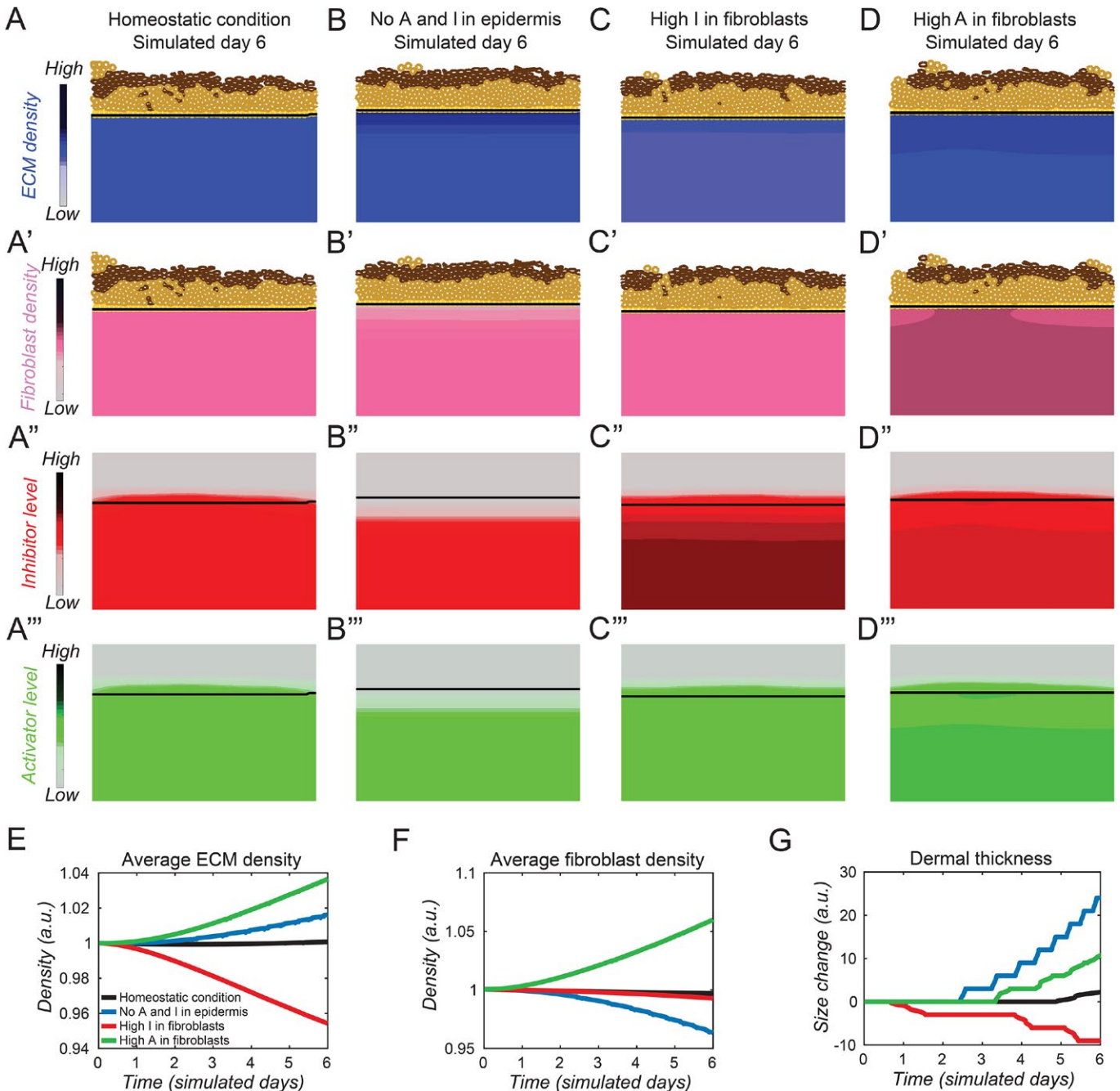


FIGURE 2 Dermal homeostasis in normal skin depends on epidermal and dermal signalling. (A-A''') Simulated ECM and fibroblast densities in unwounded skin with A and I produced both by keratinocytes and by fibroblasts. Black line denotes the position of basement membrane relative to the simulated skin surface. Fibroblast density, and I and A levels are shown in (A'), (A'') and (A'''), respectively. (B) Simulated ECM and fibroblast densities in the model where only fibroblasts produce A and I. Significantly decreased fibroblast density, and inhibitor and activator levels are shown in (B'), (B'') and (B'''), respectively. (C) Simulated ECM and fibroblast densities in the model where fibroblasts produce 10% more I relative to the homeostatic condition (high I). Corresponding fibroblast density, and inhibitor and activator levels are shown in (C'), (C'') and (C'''), respectively. (D) Simulated ECM and fibroblast densities in the model where fibroblasts produce 10% more A relative to the homeostatic condition (high A). Corresponding fibroblast density, and inhibitor and activator levels are shown in (D'), (D'') and (D'''), respectively. (E) Temporal change in average ECM density across modelling time. (F) Temporal change in average fibroblast density across modelling time. (G) Temporal change in dermal thickness, as measured by the position of basement membrane relative to the skin surface, across modelling time. Colour definitions for each line on E-G are provided on the figure. Values along X-axis are in simulated days, and values along Y-axis are in arbitrary units (a.u.)

where ϕ is the phase function representing the epidermal region ($\phi > 0$) and dermal region ($\phi < 0$). The initial condition for ϕ is the signed distance between the grid point and the interface (see Appendix S1). The velocity field v is encoded by:

$$v = -K\nabla(C - C_0) \quad (6)$$

where $C_0(x, y, t)$ is zero when (x, y) is in D , and $C_0(x, y, t)$ is $C_{stable} \neq 0$ when (x, y) is in E . C_{stable} is ECM density in the dermis under homeostatic conditions. The interface will rise up if $C > C_{stable}$ is satisfied near the interface and decrease if $C < C_{stable}$ is satisfied.

3.2 | Coupled signalling between basal keratinocytes and fibroblasts maintains dermal homeostasis in the model

To examine the effects of epidermally derived A and I on dermis stability, we varied the parameters regulating signal production by basal keratinocytes. Initially, A and I were modelled such that they are found at near-constant levels throughout D and in basal layer of E . (Figure 2A', A'''). Simulations suggest that if both basal keratinocytes

and fibroblasts produce A and I at relatively high levels and immune cells do not produce extra A because of the combined keratinocyte- and fibroblast-derived A levels are below the threshold required for immune cell activation (see Appendix S1), ECM and fibroblast densities (which serve as proxies for dermal stability) are uniformly distributed across D (Figure 2A, A'), but form an upward gradient in E (Figure S1A-A'''). The average ECM and fibroblast densities, as well as A and I levels, remained stable and did not fluctuate over a simulated timescale of 6 days (Figure 2E, F, black line). We used these simulation parameters as a baseline to represent the homeostatic condition in the following simulations, where A and I production rates and sources were perturbed.

Next, we tested the effect of disabled epidermal A and I on dermal homeostasis (Figure 2B'', B'''). This change led to near-constant levels of ECM and fibroblast densities in D , except near the epidermal-dermal interface (Figure 2B, B'), where A and I gradients shifted downwards into D (Figure S1B-B''') and over time fibroblast density decreased (Figure 2F, blue line), while ECM density increased (Figure 2E, blue line). This suggests that epidermal activator signals are primarily involved in promoting fibroblast self-renewal, while epidermal inhibitor signals prevent excessive ECM synthesis within the immediate basement membrane

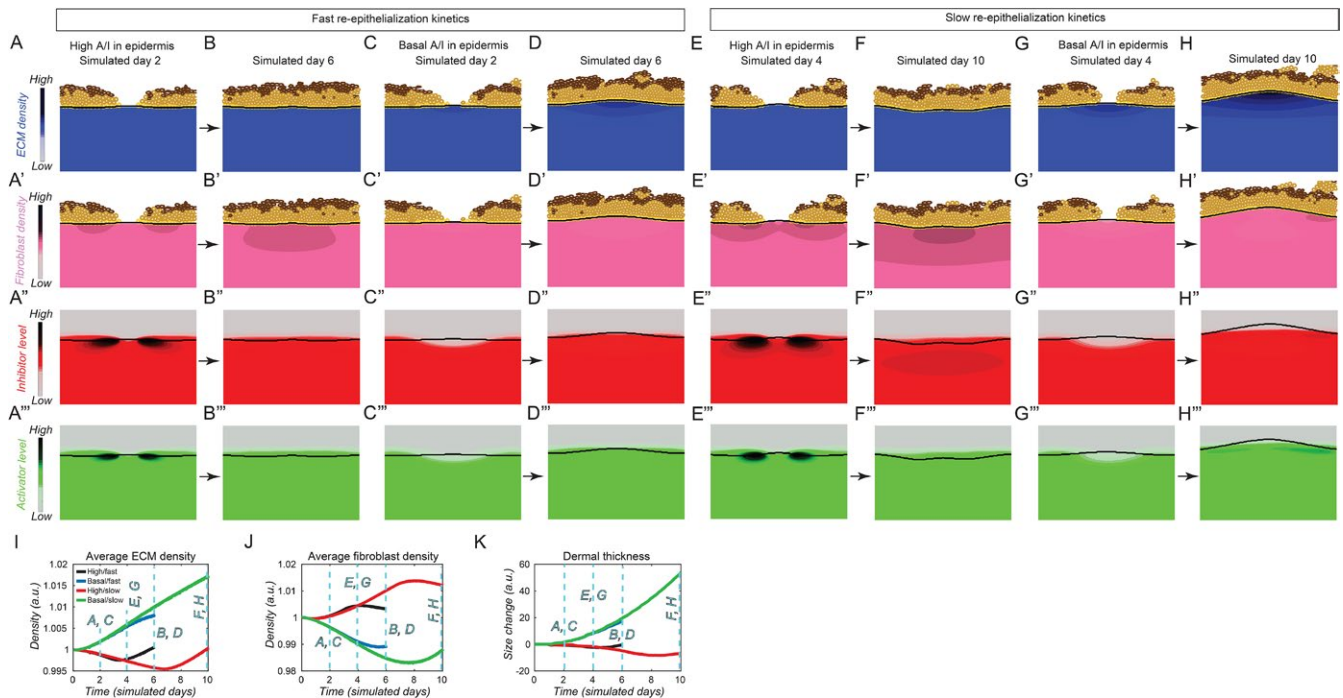


FIGURE 3 Healing outcomes of abrasion wounds depend on re-epithelialization kinetics and epidermal signal production rate. Abrasion wound healing simulations were performed using fast (A-D'') and slow re-epithelialization kinetics (E-H''). For each set of re-epithelialization kinetics, simulations were ran using "basal" (C-D'', G-H'') and "high" epidermal A/I production rates (A-B'', E-F''). For each simulated condition, ECM density (blue), fibroblast density (pink), inhibitor level (red) and activator level (green) are shown. For each simulation, two consecutive snapshots are shown: day 2 and 6 for fast re-epithelialization simulations and day 4 and 10 for slow re-epithelialization simulations. Black line on each image marks the position of basement membrane. (I) Temporal changes in average ECM density across modelling time. (J) Temporal changes in average fibroblast density across modelling time. (K) Temporal changes in dermal scar thickness across modelling time. Colour definitions for each line on I-K are provided on the figure. Values along X-axis are in simulated days, and values along Y-axis are in arbitrary units (a.u.)

microenvironment. Increase in ECM output under these signalling perturbations led to dermal thickening despite modest decrease in fibroblast density (Figure 2G, blue line). This is because in the model ECM contributes to dermal volume changes substantially more as compared to fibroblasts. This assumption is in line with the observations that ECM occupies larger proportion of a given dermal volume in adult mouse skin as compared to fibroblasts²⁵. These results also suggest that epidermal signals (primarily I) can supplement dermal signals and contribute to maintaining dermal skin compartment in homeostasis.

Next, we modelled the effects of perturbed dermal signalling. We varied the production rate of A or I in fibroblasts to two opposite extremes and simulated changes in ECM, fibroblast density and dermal thickness as measures of dermal stability. Simulation results suggest that when the production rate of I in fibroblasts is increased by more than 10% in the upper *D* compartment (Figure 2C''), fibroblast density modestly decreased and ECM production significantly decreased (Figure 2C, C'), and continued to decrease over the entire simulation period (Figure 2E, F, red lines). As expected, these changes resulted in continuously reducing dermal thickness (Figure 2G, red line). On the other hand, when the production rate of A in fibroblasts is increased by more than 10% (Figure 2D''), densities of ECM and fibroblasts as well as dermal thickness increased (Figure 2D, 2D'), and these changes continued over the simulated time (Figure 2E–G,

green lines). Together, these modelling results suggest that both epidermal and dermal sources for A and I signals and their balance are likely necessary for dermal homeostasis.

3.3 | Increased signalling and fast re-epithelialization kinetics are essential for scar-free healing in simulated epidermal abrasion wounds

Next, we asked how A and I signals may regulate dermal repair during wound healing. First, we modelled healing of epidermal abrasion wounds. Epidermal abrasions mainly heal by re-epithelialization, and no dermal scar typically forms⁴⁷. We carried out several simulations in which basal and suprabasal keratinocytes are stripped, while dermal fibroblasts and ECM remain intact (Figure S2A, B; see Appendix S1 for modelling details). We modelled two parameter kinetics that allow for “fast” and “slow” re-epithelialization in order to simulate kinetics of normal and delayed wound healing, respectively, and evaluated their effects on dermal homeostasis during and after re-epithelialization (Figure 3). Both re-epithelialization kinetics were modelled under “basal” (ie unchanged) and “high” (ie increased) epidermal A/I production rates (Figure S3; see Appendix S1). We also assumed that immediately after epidermal abrasion, A/I levels in the wound area drop below normal levels due to loss of keratinocytes, which function as the source for signals (Figure S2C, D).

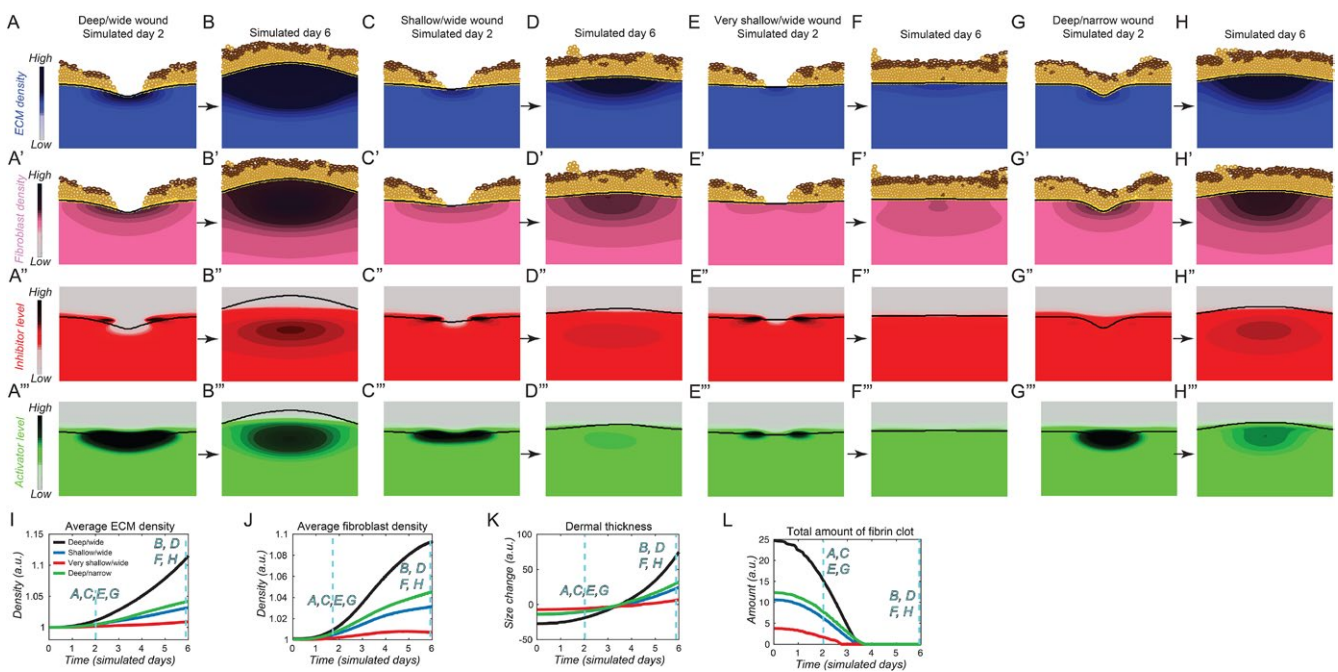


FIGURE 4 Healing outcomes of dermal wounds depend on wound geometry and fibrin clot density. All dermal wound healing simulations shown on this figure were performed using high-density fibrin clot condition. See Figure S10 for low-density fibrin clot condition. The following wound geometries were compared: (A–B'') deep and wide wounds, (C–D'') shallow and wide wounds, (E–F'') very shallow and wide wounds, and (G–H'') narrow and deep wounds. For each simulation, two consecutive snapshots are shown: day 2 and 6. Black line on each image marks the position of basement membrane. (I) Temporal changes in average ECM density across modelling time. (J) Temporal changes in average fibroblast density across modelling time. (K) Temporal changes in dermal scar thickness across modelling time. (L) Degradation dynamics of the fibrin clot across modelling time. Colour definitions for each line on I–L are provided on the figure. Values along X-axis are in simulated days, and values along Y-axis are in arbitrary units (a.u.)

First, we simulated the effects of unchanged vs increased A/I epidermal signalling under fast re-epithelialization kinetics (Figure 3A–D^{'''}). Under basal signalling conditions, A/I levels were normal at the wound edges but dropped directly beneath the epidermal wound (Figure 3C^{''}, C^{'''}). Under these simulated conditions, wound re-epithelialization was accompanied by an increase in dermal thickness (Figure 3K, blue line), an outcome that is unusual for epidermal abrasions. This is underlined by an increased ECM deposition (Figure 3D and 3I, blue line), which is the consequence of sustained lower I levels. Density of fibroblasts experienced a modest reduction (Figure 3J, blue line), opposite to ECM changes. This is also an unusual outcome, and it is driven by the disproportionally higher sensitivity of ECM production to I vs A. In contrast, when epidermal A/I levels were allowed to increase after abrasion injury (Figure 3A['], A^{''}), dermal thickness of re-epithelialized wounds did not significantly change compared to homeostatic pre-wounding state (Figure 3K, black line)—a more biologically realistic outcome. Underlying this dermal compartment behaviour in the model were near-normal fibroblast density (Figure 3J, black line) and ECM density (Figure 3I, black line). These modelling results suggest that rapid increase in A/I production by the wound edge keratinocytes is likely necessary to compensate for the loss of normal A/I levels due to epidermal injury and for eventual scar-free healing of epidermal abrasions.

Next, we modelled healing of epidermal abrasion wounds under the conditions of slow re-epithelialization kinetics, designed to simulate chronic wound healing (see Appendix S1). When modelling combined slow re-epithelialization with basal A/I production levels (Figure 3G–H^{'''}), post-injury ECM deposition (Figure 3I, green line) and dermal scarring became exacerbated (Figure 3K, green line). Interestingly, when modelling combined slow re-epithelialization with increased rate of A/I production (Figure 3E–F^{'''}), delayed re-epithelialization kinetics triggered basal keratinocytes into a state of sustained elevated production of A (Figure 3E^{'''}) and I (Figure 3E^{''}). In turn, such chronically high A/I levels resulted in dermis in and around the wound area to overproduce fibroblasts and decrease ECM (Figure 3I and 3J, red lines), causing modest, albeit abnormal decrease in dermal thickness over simulated time (Figure 3K, red line). Dichotomous behaviour of fibroblasts and ECM in this simulation is driven by higher sensitivity to changes in A and I, respectively. Taken together, our simulations indicate that proper closure of epidermal abrasion wounds and return of injured skin to near-normal homeostasis require both rapid re-epithelialization and increase in epidermal signalling.

3.4 | Simulating fibrin clot density and different wound geometries predicts their effects on the type and thickness of dermal scar

Previous studies showed that physiological inflammatory processes are necessary to achieve normal full-thickness wound repair, while abnormal inflammation levels may lead to pathological scarring⁴⁸. Important components of the inflammation phase of wound healing are diverse immune cell types⁴⁹ and the formation of a fibrin clot⁵⁰. Fibrin clot is initiated by the activation and aggregation of platelets,

and platelets release α -granule content, containing mitogenic and chemotactic growth factors important for wound healing⁵¹. Among these platelet-derived growth factors is TGF β 1²⁰, which functions as a positive regulator of ECM deposition⁵². Therefore, in our modelling, we incorporated the effect of immune cell-derived and fibrin clot-derived putative activator (modelled as A) on healing of full-thickness dermal wounds (Figure S4). We assumed that fibrin clot forms in the wound bed region during the transition between hemostasis and inflammation phases (the starting point of our simulations) and that it can have high density or be defective (ie low density) (Figure S5). We also assumed that fibrin clot serves as a “passive” source for A signal that diffuses through D and E compartments, acts on dermal components and degrades over time (Figure 4L, Figure S6). For the immune cells, we assumed that they serve as an “active” source for A, but that they produce A only when A levels are already above homeostatic. Naturally, this results in transient activation of immune cells near the wound edge and fibrin clot—the site of elevated A (Figures S7, S8).

We ran a series of simulations, starting with dermal wounds that are deep and wide (Figure S9A), imitating large excisional wounds, and that form high-density fibrin clot (Figure 4A–B^{'''}). Under these conditions, A in the wound bed reached high level (Figure 4A^{'''}), including from immune cells (Figure S7A), triggering fibroblast hyperproliferation in and around the wound (Fig 4A['], B['], J, black line). Fibroblast overproduction was accompanied by ECM overproduction (Fig 4A, B, I, black line), and the resulting scar became prominently raised and hypertrophic-like (Figure 4K, black line). Importantly, although fibrin clot decayed to zero only after three simulated days (Figure 4L, black line), signalling effects of clot-derived A on ECM deposition and fibroblast density persisted beyond that period. This is because expanding fibroblasts overtook as the dominant source of excessive A production (Figure 4B^{'''}) and immune cells continued to produce A beyond day 3 (Figure S7I, black line). Confirming these findings about fibrin clot was simulation of deep and wide wounds with defective, low-density fibrin clot (Figure S10A, B^{'''}). Under low-density clot conditions, signalling levels for A and I in and around wound bed remained relatively low (Figure S10A['], A^{'''}) and fibroblast density decreased (Figure S10J, black line), while that of ECM remained almost unchanged (Figure S10I, black line). Consequently, dermal thickness recovery dynamics were slow, such that raised scar did not develop and, instead, healed wounds acquired depressed, hypotrophic-like appearance.

Next, we modelled the effects of wound geometries on wound healing, comparing deep and wide wounds with: (a) shallow and wide, (b) very shallow and wide, and (c) deep and narrow wounds (Figure S9). Under high fibrin clot conditions, wounds of all sizes healed with raised scars of varying degree (Figure 4K) that had increased ECM density (Figure 4I) and increased fibroblast density (Figure 4J). This was underlined by increased A/I levels (Figure 4), including increased A from immune cells (Figure S7), and depended on initial high A levels originating from high-density clot. At the same time, prominent size-dependent differences were observed. Simulations suggest that the degree of dermal scarring strongly correlates with the wound's

depth rather than its width. Indeed, deep and narrow wounds (Figure 4G–H^{'''}) resulted in higher degree of scarring as compared to very shallow but wide wounds (Figure 4E–F^{'''}, K, green vs red line).

Interestingly, the above correlations between wound size and scarring outcome were altered under low-density fibrin clot conditions. Wounds of all sizes acquired depressed, hypotrophic-like appearance (Figure S10K), with scars resulting from deep wounds showing decreased fibroblast density (Figure S10J). At the signalling level, compared to high-density clot wounds, simulated low-density clot wounds quickly restored A/I levels to pre-wounding state (Figure S10).

Lastly, as proof of principle of the model's scalability, we simulated healing of deep and wide wounds with dense fibrin clot with the version of the model that contains two activators: A_1 that only stimulates ECM production and A_2 that only stimulates fibroblast proliferation (Figure S11). We tested the dependency of ECM and fibroblasts on fibrin clot-derived activator by assigning the clot to contain only A_1 (Figure S12, yellow lines) or A_2 (Figure S12, green lines). Simulations showed that fibroblast density highly depended on its activator A_2 (Figure S12B), but that lack of A_1 can be largely compensated by A_2 for ECM production (Figure S12A). This result lays the framework for modelling more complex wound healing scenarios in the future.

4 | DISCUSSION

In this work, we describe new hybrid mathematical model designed to study the effects of epidermal-dermal interactions on the molecular and cellular dynamics, and outcomes of skin wound healing. Our simulations suggest that putative activator and inhibitor signalling factors produced both in the epidermis and in the dermis are important for proper wound repair. If either of these signalling sources were perturbed in the model, dermal homeostasis and repair became altered, underlined by the defects in maintenance and restoration of ECM and fibroblast densities. For example, our model predicts how different signalling regimes affect the degree of skin scarring in the scenario when wound closure kinetics are perturbed. In the context of epidermal abrasion injuries, the ability of basal keratinocytes to rapidly increase the production of A and I over the baseline homeostatic levels was predicted to be critical for preventing skin scarring in fast re-epithelializing wounds and to minimize scarring in wounds with defective re-epithelialization, that simulates chronic epidermal wounds.

Our simulations also make several predictions regarding the effects of geometry and fibrin clot in dermal wounds. First, modelling results suggest that dermal wounds of all geometries heal by forming scar tissue that differs in its ECM and fibroblast compositions compared to unwounded skin. This is consistent with the available experimental and clinical data that adult partial-thickness and full-thickness wounds repair by scarring⁵³. Second, wide but shallow simulated wounds—an equivalent of superficial partial-thickness dermal wounds—repaired with smaller scars as compared to deep

wounds of different width, an equivalent of deep partial-thickness and full-thickness dermal wounds. Indeed, this modelling prediction is broadly consistent with the available experimental and clinical data. Superficial dermabrasion wounds, even when relatively wide, typically repair with no noticeable scar⁵⁴, while deep, full-thickness wounds even when relatively narrow, such as full-thickness incisional surgical wounds, repair with visible scars⁵⁵. Third, simulations suggest strong effects of fibrin clot on the trajectories and healing outcomes of dermal wounds. Clot density had the strongest effect on the simulated repair of deep wounds, with high-density clots causing distinctly raised, hypertrophic-like scars, while deficient, low-density clots causing somewhat depressed, hypotrophic-like scars. The initial clot density had progressively decreasing influence on the healing outcomes of shallow wounds. In our model, the effect of clot is mediated by the amount of activator that it releases, with dense clots releasing larger activator quantities. Indeed, fibrin clots contain platelet-derived growth factors and recent proteomic studies started to define their composition^{56,57}. Our modelling predictions warrant new study on the effect of fibrin clot in the animal model for wound healing, where clot formation can be regulated.

From the mathematical perspective, our model provides several advantages. Discrete nature of the epidermal compartment enables to model behaviour of individual keratinocytes, including cell proliferation, migration and signal production. Within its current framework, the model can be easily adjusted to incorporate additional epithelial cell types, such as hair follicle and/or sweat gland cell types. The model accounts for dermal compartment dynamics using continuum description, which eliminates the need for a substantially more complex and computation cost-heavy discrete description. Additional components, as shown with immune cells and two activator species, can be relatively easily added into the current model of the dermal compartment without having to fundamentally change it. Our model also implicitly considers the epidermal (E) and dermal compartments (D) and the Ω boundary between them via phase function, so that a uniform mesh can be used for both E and D . This eliminates the necessity of generating two separate meshes for E and D in order to achieve sharp compartment boundary. This approach can be applied to modelling additional sharp boundaries within the skin, such as hair follicle/dermal boundary.

In terms of its limitations, our model does not consider potential heterogeneity in skin fibroblast populations, and the possibility that different fibroblast subtypes can respond differently to signalling cues and exert distinct effects on wound healing. Indeed, several recent studies have identified distinct populations of mouse skin fibroblasts with distinct roles in ECM deposition during development and wound healing^{10,37,58–61}. Rinkevich et al. identified two populations of mouse skin fibroblasts: *En1* (Engrailed homeobox 1)-negative and *En1*-positive cells. The former are abundant during skin development, and the latter increase in numbers late in adulthood and predominantly deposit collagen and remodel ECM during wound healing⁶⁰. Developmental change in *En1*-positive vs *En1*-negative fibroblast abundance affects scarring outcomes in skin wounding experiments⁵⁹. Driskell et al. showed that during mouse skin

development, two distinct fibroblast types differentially contribute to the formation of the upper papillary and lower reticular dermal layers⁵⁸. Moreover, during wound healing, reticular fibroblasts populate the wound first, before papillary fibroblasts, and they deposit early ECM. Shook et al. showed that unwounded mouse skin contains three fibroblast populations, that one of them shares high similarity with *En1*-positive cells, and that their contributions to wound healing are distinct³⁷. Using single-cell RNA-sequencing, our group showed that early wound scars in mice contain as many as twelve fibroblast clusters and that they form at least three distinct fibroblast differentiation trajectories¹⁰. Drawing on the above experimental evidence for fibroblast heterogeneity, it will be of interest to incorporate it into wound healing models.

Indeed, a recently reported mathematical model of wound healing that utilized Cellular Potts model accounted for two fibroblast subtypes—proliferative and collagen-producing fibroblasts²⁵. In the model, the switch between two fibroblast types was positively regulated by ECM and was required to achieve dermal scar maturation. Our model herein accounts only for one type of dermal fibroblasts, and ECM production is controlled by putative activator and inhibitor factors with ECM feedback onto both, rather than by a fibroblast state switch. We posit that signalling regulations in combination with uncoupled ECM and fibroblast components within the context of a hybrid modelling approach may afford a more precise description of fibroblast and ECM dynamics and their roles in wound healing.


Lastly, our current model does not fully recapitulate all wound healing phases. Because the model lacks blood vessel and blood flow elements, it does not reproduce the hemostasis phase. Because it contains fibrin clot and immune cells, both of which are signalling sources, the model partially reproduces the inflammation phase. Our model is best suited for studying the proliferation phase but is not fully optimized for simulating long-term scar remodelling. Additional elements with negative feedback function in ECM remodelling will be required for the model to enter new stable steady state, which would recapitulate scar tissue maturation.

Overall, our multiscale hybrid model provides a flexible and efficient computational framework to investigate epidermal-dermal interactions and their effects on wound healing. By systematically adding various biological processes or elements that are critical to wound healing, one may use such modelling framework to delineate and predict novel mechanisms that have not been previously explored using experimental approaches.

ACKNOWLEDGEMENTS

This work is supported by U01-AR073159 (to Q.N. and M.V.P.). Q.N. is supported by NIH grants R01-NS095355 and R01-GM123731, and NSF grants DMS1763272 and DMS1562176, and the Simons Foundation Grant (594598, QN). M.V.P. is supported by Pew Charitable Trust grant and NIH grants R01-AR067273 and R01-AR069653. C.F.G.-J. is supported by the University of California Irvine Chancellor's ADVANCE Postdoctoral Fellowship Program.

ORCID

Christian F. Guerrero-Juarez  <https://orcid.org/0000-0002-6245-6412>

Qing Nie  <https://orcid.org/0000-0002-8804-3368>

REFERENCES

- [1] S. A. Eming, P. Martin, M. Tomic-Canic, *Sci. Transl. Med.* **2014**;6(265):265sr266.
- [2] B. K. Sun, Z. Siprashvili, P. A. Khavari, *Science* **2014**, 346(6212), 941-945.
- [3] R. F. Diegelmann, M. C. Evans, *Front Biosci.* **2004**, 9(1), 283-289.
- [4] G. C. Gurtner, S. Werner, Y. Barrandon, M. T. Longaker, *Nature* **2008**, 453(7193), 314-321.
- [5] M. Ito, Z. Yang, T. Andl, C. Cui, N. Kim, S. E. Milar, G. Cotsarelis, *Nature* **2007**, 447(7142), 316-320.
- [6] A. M. Nelson, S. K. Reddy, T. S. Ratliff, M. Z. Hossain, A. S. Katseff, A. S. Zhu, E. Chang, S. R. Resnik, C. Page, D. Kim, A. J. Whittam, L. S. Miller, L. A. Garza, *Cell Stem Cell* **2015**, 17(2), 139-151.
- [7] D. Gay, O. Kwon, Z. Zhang, M. Spata, M. V. Plikus, P. D. Holler, M. Ito, Z. Yang, E. Treffeisen, C. D. Kim, A. Nace, X. Zhang, S. Baratono, F. Wang, D. M. Ornitz, S. E. Millar, *Nat. Med.* **2013**, 19(7), 916-923.
- [8] C. H. Lim, Q. Sun, K. Ratti, S. H. Lee, Y. Zheng, M. Takeo, W. Lee, P. Rabbani, M. V. Plikus, J. E. Cain, D. H. Wang, D. N. Watkins, S. Millar, M. M. Taketo, P. Myung, G. Cotsarelis, M. Ito, *Nat. Commun.* **2018**, 9(1), 4903.
- [9] M. V. Plikus, C. F. Guerrero-Juarez, M. Ito, Y. R. Li, P. H. Dedhia, Y. Zheng, M. Shao, D. L. Gay, R. Ramos, T. C. Hsi, J. W. Oh, X. Wang, A. Ramirez, S. E. Konopelski, A. Elzein, A. Wang, R. J. Supapannachart, H. L. Lee, C. H. Lim, A. Nace, A. Guo, E. Treffeisen, T. Andl, R. N. Ramirez, R. Murad, S. Offermanns, D. Metzger, P. Chambon, A. D. Widgeow, T. L. Tuan, A. Mortazavi, R. K. Gupta, B. A. Hamilton, S. E. Millar, P. Seale, W. S. Pear, M. A. Lazar, G. Cotsarelis, *Science* **2017**, 355(6326), 748-752.
- [10] C. F. Guerrero-Juarez, P. H. Dedhia, S. Jin, R. Ruiz-Vega, D. Ma, Y. Liu, K. Yamaga, O. Shestova, D. L. Gay, Z. Yang, K. Kessenbrock, Q. Nie, W. S. Pear, G. Cotsarelis, M. V. Plikus, *Nat. Commun.* **2019**, 10(1), 650.
- [11] J. J. Tomasek, G. Gabbiani, B. Hinz, C. Chaponnier, R. A. Brown, *Nat. Rev. Mol. Cell Biol.* **2002**, 3(5), 349-363.
- [12] D. J. Whitby, M. W. Ferguson, *Development* **1991**, 112(2), 651-668.
- [13] M. Xue, C. J. Jackson, *Adv. Wound Care (New Rochelle)*. **2015**;4(3):119-136.
- [14] W. L. Garner, *Plast. Reconstr. Surg.* **1998**, 102(1), 135-139.
- [15] Z. Wang, Y. Wang, F. Farhangfar, M. Zimmer, Y. Zhang, *PLoS ONE* **2012**, 7(7), e40951.
- [16] S. Werner, T. Krieg, H. Smola, *J. Invest. Dermatol.* **2007**, 127(5), 998-1008.
- [17] A. B. Roberts, M. B. Sporn, R. K. Assoian, J. M. Smith, N. S. Roche, L. M. Wakefield, U. I. Heine, L. A. Liotta, V. Falanga, J. H. Kehrl, *Proc Natl Acad Sci U S A.* **1986**, 83(12), 4167-4171.
- [18] M. W. Ferguson, S. O'Kane, *Philos. Trans. R. Soc. Lond. B Biol. Sci.* **2004**, 359(1445), 839-850.
- [19] S. O'Kane, M. W. Ferguson, *Int. J. Biochem. Cell Biol.* **1997**, 29(1), 63-78.
- [20] B. L. Eppley, J. E. Woodell, J. Higgins, *Plast. Reconstr. Surg.* **2004**, 114(6), 1502-1508.
- [21] J. A. Sherratt, J. D. Murray, *Proc Biol Sci.* **1990**, 241(1300), 29-36.
- [22] B. D. Cumming, D. L. McElwain, Z. Upton, *J. R. Soc. Interface* **2010**, 7(42), 19-34.
- [23] S. McDougall, J. Dallon, J. Sherratt, P. Maini, *Philos Trans A Math Phys Eng Sci.* **1843**, 2006(364), 1385-1405.

- [24] J. T. Daub, R. M. Merks, *Bull. Math. Biol.* **2013**, 75(8), 1377-1399.
- [25] E. Rognoni, A. O. Pisco, T. Hiratsuka, K. H. Sipilä, J. M. Belmonte, S. A. Mobasser, C. Philippes, R. Dilão, F. M. Watt, *Mol. Syst. Biol.* **2018**, 14(8), e8174.
- [26] S. N. Menon, J. A. Flegg, S. W. McCue, R. C. Schugart, R. A. Dawson, D. L. McElwain, *Proc Biol Sci.* **2012**, 279(1741), 3329-3338.
- [27] F. J. Vermolen, E. Javierre, *J. Math. Biol.* **2012**, 65(5), 967-996.
- [28] H. Du, Y. Wang, D. Haensel, B. Lee, X. Dai, Q. Nie, *PLoS Comput. Biol.* **2018**, 14(2), e1006006.
- [29] T. J. Newman, *Mathematical Biosciences and Engineering.* **2005**, 2(3), 613-624.
- [30] A. Gord, W. R. Holmes, X. Dai, Q. Nie, *J. R. Soc. Interface* **2014**, 11(99), 20140631.
- [31] T. Hillen, K. J. Painter, *J. Math. Biol.* **2009**, 58(1-2), 183-217.
- [32] S. Osher, R. P. Fedkiw, *J. Comput. Phys.* **2001**, 169(2), 463-502.
- [33] K. W. Finson, S. McLean, G. M. Di Guglielmo, A. Philip, *Adv. Wound Care (New Rochelle)*. **2013**, 2(5), 195-214.
- [34] R. Hosokawa, K. Nonaka, M. Morifuji, L. Shum, M. Ohishi, *J. Dent. Res.* **2003**, 82(7), 558-564.
- [35] S. Barrientos, O. Stojadinovic, M. S. Golinko, H. Brem, M. Tomic-Canic, *Wound Repair Regen.* **2008**, 16(5), 585-601.
- [36] Y. Liu, Y. Li, N. Li, W. Teng, M. Wang, Y. Zhang, Z. Xiao, *Sci. Rep.* **2016**, 6, 32231.
- [37] Shook B. A., Wasko R. R., Rivera-Gonzalez G. C., E. Salazar-Gatzimas, F. López-Giráldez, B. C. Dash, A. R. Muñoz-Rojas, K. D. Aulman, R. K. Zwick, V. Lei, J. L. Arbiser, K. Miller-Jensen, D. A. Clark, H. C. Hsia, V. Horsley, *Science.* **2018**;362(6417):eaar2971.
- [38] V. Falanga, L. Zhou, T. Yufit, *J. Cell. Physiol.* **2002**, 191(1), 42-50.
- [39] H. Murata, L. Zhou, S. Ochoa, A. Hasan, E. Badiavas, V. Falanga, *J. Invest. Dermatol.* **1997**, 108(3), 258-262.
- [40] K. Y. Wang, S. Yamada, H. Izumi, M. Tsukamoto, T. Nakashima, T. Tasaki, X. Guo, H. Uramoto, Y. Sasaguri, K. Kohno, *PLoS ONE* **2018**, 13(3), e0195156.
- [41] E. J. Hamburg, R. P. Atit, *J. Invest. Dermatol.* **2012**, 132(10), 2469-2472.
- [42] A. Akhmetshina, K. Palumbo, C. Dees, C. Bergmann, P. Venalis, P. Zerr, A. Horn, T. Kireva, C. Beyer, J. Zwerina, H. Schneider, A. Sadowski, M. O. Riener, O. A. MacDougald, O. Distler, G. Schett, J. H. Distler, *Nat. Commun.* **2012**, 3, 735.
- [43] J. Wei, D. Melichian, K. Komura, M. E. Hinchcliff, A. P. Lam, R. Lafyatis, C. Gottardi, O. A. MacDougald, J. Varga, *Arthritis Rheum.* **2011**, 63(6), 1707-1717.
- [44] T. Iwayama, C. Steele, L. Yao, M. G. Dozmorov, D. Karamichos, J. D. Wren, L. E. Olson, *Genes Dev.* **2015**, 29(11), 1106-1119.
- [45] L. E. Olson, P. Soriano, *Dev. Cell* **2009**, 16(2), 303-313.
- [46] T. Hiragun, E. Morita, T. Tanaka, Y. Kameyoshi, S. Yamamoto, *J. Invest. Dermatol.* **1998**, 111(2), 213-217.
- [47] J. D. Stroncek, W. M. Reichert, *Indwelling neural implants: strategies for contending with the in vivo environment*, CRC Press, Boca Raton, FL, **2008**:3-40.
- [48] S. H. Kwon, G. C. Gurtner, *Exp. Dermatol.* **2017**, 26(2), 133-134.
- [49] S. A. Eming, T. Krieg, J. M. Davidson, *J. Invest. Dermatol.* **2007**, 127(3), 514-525.
- [50] N. S. Greaves, K. J. Ashcroft, M. Baguneid, A. Bayat, *J. Dermatol. Sci.* **2013**, 72(3), 206-217.
- [51] A. T. Nurden, P. Nurden, M. Sanchez, I. Andia, E. Anitua, *Front Biosci.* **2008**, 13, 3532-3548.
- [52] Wells R. G., Discher D. E., *Sci. Signal.* **2008**;1(10):pe13.
- [53] I. Pastar, O. Stojadinovic, N. C. Yin, H. Ramirez, A. G. Nusbaum, A. Sawaya, S. B. Patel, L. Khalid, R. R. Lsseroff, M. Tomic-Canic, *Adv. Wound Care (New Rochelle)*. **2014**, 3(7), 445-464.
- [54] C. D. Marshall, M. S. Hu, T. Leavitt, L. A. Barnes, H. P. Lorenz, M. T. Longaker, *Adv. Wound Care (New Rochelle)*. **2018**, 7(2), 29-45.
- [55] J. R. Hinshaw, E. R. Miller, *Arch. Surg.* **1965**, 91(4), 658-670.
- [56] A. Stachowicz, J. Siudut, M. Suski, R. Olszanecki, R. Korbut, A. Undas, J. R. Wiśniewski, *Clin. Proteomics* **2017**, 14, 38.
- [57] E. Anitua, R. Prado, M. Azkargorta, E. Rodriguez-Suárez, I. Iloro, J. Casado-Vela, F. Elortza, G. Orive, *J. Tissue Eng. Regen. Med.* **2015**, 9(11), E1-E12.
- [58] R. R. Driskell, B. M. Lichtenberger, E. Hoste, K. Kretzschmar, B. D. Simons, M. Charalambous, S. R. Ferron, Y. Herault, G. Pavlovic, A. C. Ferguson-Smith, F. M. Watt, *Nature* **2013**, 504(7479), 277-281.
- [59] D. Jiang, D. Correa-Gallegos, S. Christ, A. Stefanska, J. Liu, P. Ramesh, V. Rajendran, M. M. De Santis, D. E. Wagner, Y. Rinkevich, *Nat. Cell Biol.* **2018**, 20(4), 422-431.
- [60] Y. Rinkevich, G. G. Walmsley, Hu M. S., Z. N. Maan, A. M. Newman, M. Drukker, M. Januszzyk, G. W. Karpitz, G. C. Gurtner, H. P. Lorenz, I. L. Weissman, M. T. Longaker, *Science.* **2015**;348(6232):aaa2151.
- [61] C. Philippes, S. B. Telerman, B. Oules, A. O. Pisco, T. J. Shaw, R. Elgueta, G. Lombardi, R. R. Driskell, M. Soldin, M. D. Lynch, F. M. Watt, *J. Invest. Dermatol.* **2018**, 138(4), 811-825.

SUPPORTING INFORMATION

Additional supporting information may be found online in the Supporting Information section at the end of the article.

Table S1 Parameter values for epidermal discrete model. Parameters are included for subcellular element method (SEM), cell cycle, cell self-renewal probability, cell growth rate, cell decay rate, selective adhesion, and cell migration.

Table S2 Parameter values for dermal continuum model. Parameters for fibroblasts, ECM, immune cells, activator, inhibitor and fibrin clot density are included.

Table S3 Parameter values for wound size and fibrin clot density.

Appendix S1 Supplementary Information.

How to cite this article: Wang Y, Guerrero-Juarez CF, Qiu Y, et al. A multiscale hybrid mathematical model of epidermal-dermal interactions during skin wound healing. *Exp Dermatol.* 2019;28:493-502. <https://doi.org/10.1111/exd.13909>